

# Adaptive energy reference for machine-learning models of the electronic density of states

Wei Bin How, Sanggyu Chong, Federico Grasselli, Kevin K. Huguenin-Dumittan, and Michele Ceriotti\*  
*Laboratory of Computational Science and Modeling, IMX,  
École Polytechnique Fédérale de Lausanne, Lausanne 1015, Switzerland*

The electronic density of states (DOS) provides information regarding the distribution of electronic states in a material, and can be used to approximate its optical and electronic properties and therefore guide computational material design. Given its usefulness and relative simplicity, it has been one of the first electronic properties used as target for machine-learning approaches going beyond interatomic potentials. A subtle but important point, well-appreciated in the condensed matter community but usually overlooked in the construction of data-driven models, is that for bulk configurations the absolute energy reference of single-particle energy levels is ill-defined. Only energy differences matter, and quantities derived from the DOS are typically independent on the absolute alignment. We introduce an adaptive scheme that optimizes the energy reference of each structure as part of training, and show that it consistently improves the quality of ML models compared to traditional choices of energy reference, for different classes of materials and different model architectures. On a practical level, we trace the improved performance to the ability of this self-aligning scheme to match the most prominent features in the DOS. More broadly, we believe that this work highlights the importance of incorporating insights into the nature of the physical target into the definition of the architecture and of the appropriate figures of merit for machine-learning models, that translate in better transferability and overall performance.

## I. INTRODUCTION

The electronic density of states (DOS) characterizes the distribution of available energy states for electrons and can be used to investigate many properties of a material [1, 2], such as its electrical conductivity and optical properties. Hence, the DOS can be useful for material discovery and design by providing a tool to screen promising material candidates. Given the good balance between accuracy and cost, the DOS is often computed using density functional theory (DFT), where the electrons are treated as non-interacting fermions and their interactions are modelled by a self-consistent mean-field potential. Even within this approximate treatment, the calculation of the DOS scales cubically with the number of electrons in the system [3]. Hence, studying the DOS of large and complex systems is still prohibitively difficult.

Recently, machine learning (ML) has been shown to be a promising alternative approach to circumvent the expensive DFT calculations for large systems [4–10]. Over the past two decades, there has been significant developments in the integration of machine learning in computational materials science, ranging from the development of new features [11–14] to different model architectures [15–17] to predict various material properties with high accuracy and low cost. Aside from the prediction of material properties, there has also been significant advancements in evaluating the reliability of these methods [18, 19] and improving the efficiency of machine learning via dimensionality reduction of the feature space [20–24].

Even though early efforts in this field focused on predicting the interatomic potentials [25], more recently there have been works geared towards modeling of the electronic structure, including the DOS. Broderick and Rajan demonstrated that the prediction of the DOS can be done by decomposing it using principal component analysis (PCA) and subsequently predicting the components using elemental descriptors [26]. This approach was then further extended to metal alloys by Yeo *et al.* and applied together with graph neural networks to metallic nanoparticles by Bang *et al.* [27, 28]. Another approach was proposed by del Rio and Chandrasekeran *et al.*, using multilayer perceptrons (MLPs) to effectively learn and predict the DOS discretized on an energy grid [3, 29]. Similarly, this approach has also been extended to more complex models such as graph neural networks and attention networks [30, 31]. Furthermore, Ben Mahmoud *et al.* performed the prediction of the DOS, both on the discretized energy grid and the principal components, using kernel ridge regressors [32].

One detail that has been often overlooked in the previous works is the lack of an absolute electronic energy reference in the quantum mechanical calculations of infinite bulk systems [33]. Typical quantum chemical softwares define the energy reference as the average Hartree potential in the cell [34] based on:

$$V_H = \frac{1}{\Omega} \int_{cell} d^3\mathbf{r} V(\mathbf{r}). \quad (1)$$

where  $V(\mathbf{r})$  represents the Hartree potential at point  $\mathbf{r}$ , and  $\Omega$  represents the volume of the unit cell. Due to the conditionally convergent nature of the potentials in an infinite bulk system, the average Hartree potential is usually ill-defined for an infinite bulk system [35].

This issue is very well recognized in condensed-matter

\* michele.ceriotti@epfl.ch

modeling, and several approaches have been developed to alleviate it by defining an external energy reference within the system. One class of methods attempts to define the vacuum potential within the cell. This can be achieved by creating a surface by introducing sufficient amounts of empty space into the unit cell for the potential to converge to a constant vacuum potential [36]. For sufficiently porous systems, one can define the vacuum potential as the spherical average of the electrostatic potential at the center of the pore [37]. An alternative approach is to build a cluster model of the lattice embedded in the potential of the periodic crystal [38]. By virtue of being a cluster model, the calculation will include a vacuum region where the energy reference can be defined. Nevertheless, these methods only work well for specific system types and cannot be generalized to all bulk systems. Additionally, it is important to note that a “true” external energy reference for an infinite bulk systems is still ill-defined and these approaches only serve to provide a proxy for it. Consequently, only the quantities that are independent of the energy reference can be compared against experimental observables [39].

Hence, the energy reference chosen for the DOS is arbitrary and inconsequential as long as the quantities derived are independent of it. However, most ML methods do not treat the DOS in a way that is independent of the energy reference, but instead employ either the the average Hartree potential,  $V_H$ , or the Fermi level,  $E_F$ , of the system as the energy reference of each structure in the dataset. Therefore, the energy reference chosen for each structure can have an impact on the performance of a ML model. For instance, an energy reference that is poorly defined across the dataset can lead to common spectral features being manifested at different energy values for each structure. This artificially increases the complexity of the dataset and can introduce discontinuities in the mapping between descriptors and targets that hamper model learning.

In this work, we present a machine-learning framework that treats the energy reference of the DOS of *each* structure in the dataset as an optimizable parameter. The framework is demonstrated on descriptors built on the smooth overlap of atomic positions (SOAP) power spectrum using both linear and nonlinear models. We showcase the effectiveness of this approach in improving the performance of machine learning predictions of the DOS and its derived quantities. Four datasets of varying complexity and elemental compositions are used to assess the performance of this framework. For each dataset, the framework is compared against the other commonly used energy references,  $V_H$  and  $E_F$ . We show that treating the energy reference of the DOS as an optimizable parameter consistently leads to the best performing models for both the DOS and the observables that can be derived from it, and rationalize these results in terms of the alignment of the main spectral features of the DOS. This framework can improve the generalizability of machine learning methods for the prediction of the DOS, especially on

datasets where common spectral patterns are not well-aligned when employing conventional energy references.

## II. METHODS

Although experimentally accessible quantities derived from the DOS are independent of the energy reference, machine-learning models are typically trained and evaluated in a way that does depend on the relative alignment of the energy reference chosen for the dataset. This is seen in the mean squared error (MSE) loss function that is typically employed for MLDOS:

$$L(\mathbf{W}) = \frac{1}{N} \sum_A \int dE \left( \text{DOS}_A^Q(E) - \text{DOS}_A^W(E) \right)^2. \quad (2)$$

In this loss function,  $N$  represents the number of structures in the dataset,  $\mathbf{W}$  represents the parameters of the model,  $\text{DOS}_A^Q(E)$  represents the DOS obtained from quantum chemical calculations for structure  $A$ , and  $\text{DOS}_A^W(E)$  represents the DOS predicted by the model with parameter  $\mathbf{W}$ . Here, changing the energy reference of  $\text{DOS}_A^Q(E)$  by replacing  $E$  with  $E + \Delta$ , where  $\Delta$  parameterizes the changes in the energy reference, would result in a different loss value.

One solution to this would be to redefine the training and evaluation metrics to be independent of the energy reference. This can be achieved by reformulating the MSE loss such that the predicted DOS is evaluated on the energy reference that minimizes the loss:

$$L(\mathbf{W}) = \frac{1}{N} \sum_A \min_{\Delta_A} \left[ \int dE \left( \text{DOS}_A^Q(E + \Delta_A) - \text{DOS}_A^W(E) \right)^2 \right]. \quad (3)$$

In this redefined MSE,  $\Delta_A$  is a parameter that shifts the energy reference of  $\text{DOS}_A^Q$ , and is chosen to be the value that minimizes the MSE for the DOS of structure  $A$  predicted by the model.

Although Eq. (3) is a better metric to evaluate the quality of models trained, implementing it as a loss to drive the training process results in significantly longer training times (see Supporting Information). In view of this, our approach for DOS learning instead treats  $\Delta_A$  of the structures in the training dataset as a parameter to be optimized alongside the model parameters during model training, corresponding to a “self-aligning” loss:

$$L(\mathbf{W}, \Delta) = \frac{1}{N} \sum_A \int dE \left( \text{DOS}_A^Q(E + \Delta_A) - \text{DOS}_A^W(E) \right)^2. \quad (4)$$

A schematic that shows the effect of optimizing  $\Delta_A$  for a self-aligning loss is found in Fig. 1. By introducing  $\Delta_A$  as an optimizable parameter, the model is free to adjust the energy reference while training. This way, the loss of the model would not be artificially inflated by a choice of energy reference that has poor alignment between the structures in the dataset, which is not physically relevant. As a result, the weights of the model would be more responsive to the loss induced by the physically meaningful spectral details of the DOS. We show in the Supporting Information that the joint optimization of  $\Delta_A$  and  $\mathbf{W}$  through the loss (4) achieves similar results to the optimization of  $\mathbf{W}$  using loss (3) at much shorter training times. Additionally, the joint optimization framework can be easily integrated into existing DOS ML workflows via a simple modification of the model training loop (Section II A). The remainder of this section discusses the structure of the model and the construction of the ML targets.

### A. Model Details

In this work, we employ a locality ansatz where the global DOS of a structure  $A$  is decomposed into contributions from each atomic environment,  $A_i$ :

$$\text{DOS}_A(E) = \frac{1}{N_A} \sum_{A_i \in A} \text{LDOS}_{A_i}(E), \quad (5)$$

where  $N_A$  represents the total number of atomic environments in structure  $A$  and  $\text{LDOS}_{A_i}$  represents the local contribution of environment  $A_i$  to the global DOS. Additionally, the models are constructed such that they predict the DOS values at different energy values on the grid, in a multi-target regression manner.

In order to account for differences in system sizes across the dataset, the DOS is normalized with respect to the number of atoms in the structure. The original energy reference before the shift parameter,  $\Delta$ , is applied is chosen to be  $E_F$  as it gives the best results when using a fixed reference. Furthermore, in order to only capture the relative energy references across the structures in the dataset, the mean of  $\Delta$  is subtracted out such that the mean change in energy reference across the dataset is 0 eV. For models trained without optimizing the energy reference, the loss was defined as in Eq. (2).

In this work, the new framework was deployed on both linear models and MLPs, using the SOAP power spectrum as input features. The MLPs have one hidden layer, corresponding to the size of the number of input features. Specific details about the SOAP power spectrum, model architecture and training can be found in the Supporting Information.

### B. Constructing the DOS

To construct the DOS for a bulk structure from a finite number of  $\mathbf{k}$ -points, the DOS is computed by applying Gaussian broadening to the eigenenergies:

$$\text{DOS}_A^\delta(E) = \frac{1}{N_A} \frac{2}{N_k} \sum_{n \in \text{bands}} \sum_{\mathbf{k}} g(E - \epsilon_n(\mathbf{k}) - \delta_A) \quad (6)$$

$$g(x) = \frac{1}{\sqrt{2\pi\sigma^2}} e^{-\frac{x^2}{2\sigma^2}}, \quad (7)$$

where  $\delta$  represents the energy reference used to define the dataset,  $N_A$  represents the number of atoms in the structure,  $N_k$  represents the number of  $\mathbf{k}$ -points from which the eigenenergies were computed from,  $\epsilon_n(\mathbf{k})$  represents the eigenenergy of each band,  $n$ , at different  $\mathbf{k}$ -points, and  $\sigma$  represents the Gaussian broadening parameter.

Since the energy reference for each structure is defined to be their respective cell average Hartree potentials, the eigenenergies,  $\epsilon_n(\mathbf{k})$ , are also referenced to the cell average Hartree potential by default. To obtain the DOS referenced to  $V_H$  or the Fermi level, the energy reference  $\delta$  is set to either zero or the Fermi level with respect to  $V_H$ , respectively. The Fermi level,  $E_F$ , relative to  $V_H$  is defined as follows:

$$n_{\text{val}}(A) = \int_{-\infty}^{E_F^A} dE \text{DOS}_A^H(E) \quad (8)$$

where  $n_{\text{val}}(A)$  indicates the number of valence electrons used in the DFT calculation of system  $A$ , and  $E_F^A$  is the Fermi level of structure  $A$  relative to  $V_H$ .

As the DOS is represented on a discretized energy grid, calculating the change, and the derivative, of the DOS with respect to a change in the energy reference would be computationally expensive as one would have to recalculate Eq. (6) again, for a large number of structures and eigenenergies. To tackle this, cubic Hermite splines [40] are built on the DOS, where the DOS function is represented piecewise by a third-degree polynomial that is defined by the value and first derivative at the end points of the interval. Given that the  $\Delta_A$  term in Eq. (3) and Eq. (4) is always applied on  $\text{DOS}_A^Q$  instead of  $\text{DOS}_A^W$ , the splines only need to be built once before model training.

Additionally, to evaluate the performance of the models on derived quantities of the DOS that are independent of the energy reference, secondary observables such as the  $\text{DOS}(E_F)$  and the distribution of excitations,  $X(\theta)$ , are also calculated for each structure. The equation for the distribution of excitations is defined as follows [32]:

$$X_A(\theta) = \iint dE dE' \text{DOS}_A^\delta(E) f_{\text{FD}}(E - E_F^A)|_{T=0} \quad (9)$$

$$\text{DOS}_A^\delta(E') (1 - f_{\text{FD}}(E' - E_F^A)|_{T=0}) \delta(E - E' - \theta)$$

It can be observed that  $X(\theta)$  is independent of the energy reference since the Fermi level of the system,  $E_F^A$ , acts as

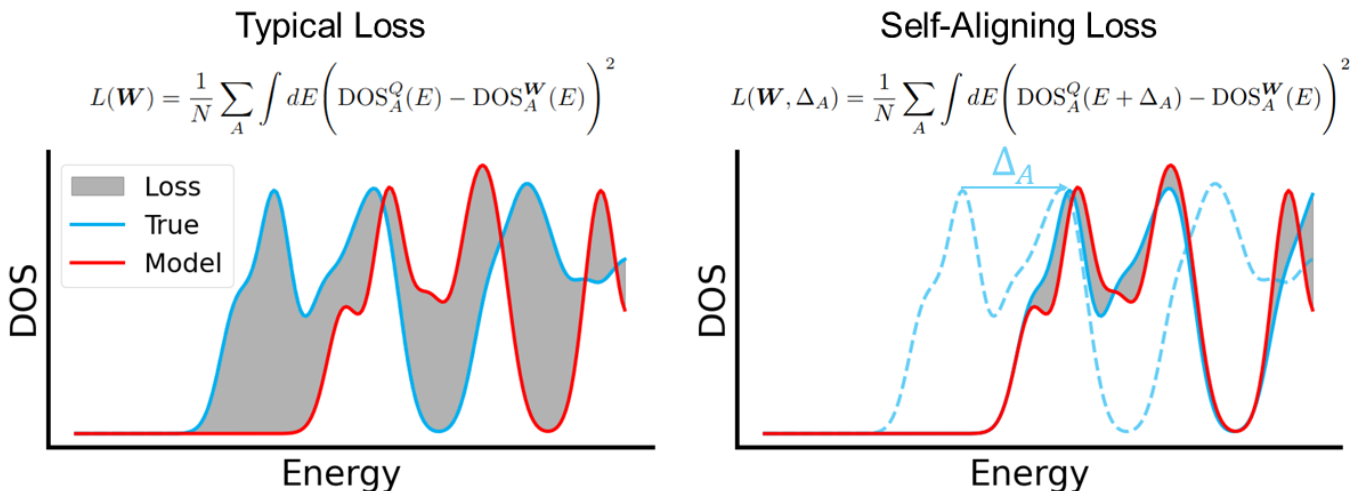


FIG. 1. A schematic that highlights the difference between the typical loss and the self-aligning loss in training ML models for DOS predictions.

an independent point of reference for the system. In this work, the activation energy,  $\theta$ , is defined on an energy grid ranging from 0 to 2 eV, with a 0.05 eV grid spacing.

### III. RESULTS

#### A. Datasets

A total of four datasets were used to evaluate the effectiveness of the joint optimization scheme. The first dataset comprises 927 silicon structures obtained from Bartok *et al.* [41], spanning across four different bulk phases: diamond, beta-tin, liquid and amorphous bulk, and surfaces. DFT calculations of the structures were performed using FHI-aims [34] with the parameters employed by Ben Mahmoud *et al.* [32]. The second dataset is adapted from Cheng *et al.* [42] and is composed of bulk hydrogen configurations at high pressures, including a phase transition between solid and liquid hydrogen. 20,000 structures were subselected from the entire dataset. Of the 20,000 structures, 5000 structures were obtained from ab initio molecular dynamics, and 2143 structures were selected from each of the seven iterations of the random structure search approach employed using farthest point sampling. DFT calculations of the structures were performed using Quantum Espresso [43–45] with the parameters employed by Ben Mahmoud *et al.* [46]. The third dataset is that of BaTiO<sub>3</sub>, a perovskite crystal which exhibits strong ferroelectric properties and has technological relevance [47, 48]. Four phases, rhombohedral, orthorhombic, tetragonal, and cubic, are included in the dataset. The dataset comprises of 840 structures, with 210 structures in each phase and is obtained from the NpT subset of the BaTiO<sub>3</sub> dataset built by Gigli *et al.* [49]. The last dataset is that of a Ga<sub>x</sub>As<sub>1-x</sub> binary system over a wide range of temperatures, pres-

ures, and stoichiometry in order to accurately represent the changes in the electronic behaviour of the system across the binary phase diagram. This is particularly important as GaAs is a semiconductor with excellent electronic and optical properties, lending itself applications in solar cells and photonics [50, 51]. The dataset is obtained from Imbalzano *et al.* [52] and is composed of crystalline structures, liquid phases, and various interfaces. The dataset is then recomputed at a higher level of theory to account for van der Waals interactions and a larger number of electronic bands. The computational parameters for all the datasets used are detailed in the Supporting Information.

With the exception of the hydrogen dataset, the DOS energy range spans from 1.5 eV below the lowest eigenenergy to 3 eV above the maximum Fermi level in the dataset, while the splines are defined up to 6 eV above the maximum Fermi level. Meanwhile for the hydrogen dataset, due to high  $\Delta_A$  values and high predicted  $E_F$ , the DOS energy range instead spans up to 7 eV above the maximum Fermi level and the splines are defined up to 12 eV above the maximum Fermi level. For all datasets, the DOS energy range is discretized on a grid with a spacing of 0.05 eV while that of the splines is much finer at 0.001 eV.

Each dataset is split randomly in a 7:1:2 ratio to give the training, validation and test set, respectively. Smaller subsets, taken at 25, 50 and 75 percent of the training and validation data, were also used to train the model to construct learning curves. The calculation parameters for each dataset are reported in the Supporting Information.

#### B. Evaluation of Model Performance

To assess the impact of the choice of energy reference, we evaluate the performance of each model on the DOS

| Dataset                           | Linear Models Test RMSE <sup>DOS</sup><br>[eV <sup>-0.5</sup> atom <sup>-1</sup> state] |                |          | Multilayer Perceptrons Test RMSE <sup>DOS</sup><br>[eV <sup>-0.5</sup> atom <sup>-1</sup> state] |                |          |
|-----------------------------------|---|----------------|----------|--|----------------|----------|
|                                   | V <sub>H</sub>  | E <sub>F</sub> | Adaptive | V <sub>H</sub>   | E <sub>F</sub> | Adaptive |
| Si                                | 0.05782   | 0.04281        | 0.03979  | 0.04094  | 0.03318        | 0.02988  |
| H                                 | 0.03317   | 0.02915        | 0.02683  | 0.03003  | 0.02561        | 0.02270  |
| BaTiO <sub>3</sub>                | 0.06809   | 0.02665        | 0.02255  | 0.02879  | 0.02460        | 0.01816  |
| Ga <sub>x</sub> As <sub>1-x</sub> |   | 0.2031         | 0.09932  |  | 0.1936         | 0.09687  |

TABLE I. DOS RMSE of models trained on different datasets and different energy references. The DOS RMSE is evaluated on the test set and has units of  $eV^{-0.5}atom^{-1}state$ . For Ga<sub>x</sub>As<sub>1-x</sub>, there were no models trained using the cell average Hartree Potential as the energy reference due to the high range of Fermi levels in the dataset. Additionally, due to the significant bandgap present in the structures of BaTiO<sub>3</sub> the highest occupied molecular orbital (HOMO) was used in place of E<sub>F</sub> to define the energy reference.

| Dataset                           | Multilayer Perceptrons RMSE <sup>DOS(E<sub>F</sub>)</sup><br>[eV <sup>-1</sup> atom <sup>-1</sup> state] |                |          | Multilayer Perceptrons RMSE <sup>X</sup><br>[eV <sup>-0.5</sup> atom <sup>-2</sup> state <sup>2</sup> ] |                |           |
|-----------------------------------|--|----------------|----------|---|----------------|-----------|
|                                   | V <sub>H</sub>   | E <sub>F</sub> | Adaptive | V <sub>H</sub>  | E <sub>F</sub> | Adaptive  |
| Si                                | 0.02346  | 0.02357        | 0.02011  | 0.007020  | 0.006828       | 0.006143  |
| H                                 | 0.009441   | 0.009941       | 0.007961 | 0.0008574   | 0.0009790      | 0.0008430 |
| BaTiO <sub>3</sub>                | 0.09531  | 0.14096        | 0.06288  | 0.02068   | 0.03218        | 0.01230   |
| Ga <sub>x</sub> As <sub>1-x</sub> |  | 0.03561        | 0.03622  |   | 0.02543        | 0.01370   |

TABLE II. RMSE on secondary quantities for MLP models trained on different datasets and different energy references. All RMSEs are evaluated on the test set. The RMSE for DOS(E<sub>F</sub>) has units of  $eV^{-1}atom^{-1}state$  and that of  $X$  has units of  $eV^{-0.5}atom^{-2}state^2$ . For Ga<sub>x</sub>As<sub>1-x</sub>, there were no models trained using the cell average Hartree potential as the energy reference due to the wide range of Fermi levels in the dataset. Additionally, due to the significant bandgap present in the structures of BaTiO<sub>3</sub> the HOMO was used in place of E<sub>F</sub> to define the energy reference.

and its derived quantities using the root mean squared error (RMSE), defined as the square root of the corresponding MSE value, on the test set. In order to evaluate each model in a way that is independent of the energy reference, the MSE is calculated for the energy reference that minimizes it in a manner analogous to the definition in Eq. (3):

$$\text{MSE}^{\text{DOS}}(\mathbf{W}) = \frac{1}{N} \sum_A \min_{\Delta_A} \left[ \int dE \left( \text{DOS}_A^Q(E + \Delta_A) - \frac{1}{N_A} \sum_{A_i \in A} \text{LDOS}_{A_i}^W(E) \right)^2 \right]. \quad (10)$$

The variables follow the same conventions as those used in Eq. (3). Additionally, LDOS<sub>A<sub>i</sub></sub><sup>W</sup> refers to the predicted atomic contribution to the DOS of atomic environment A<sub>i</sub>, as in Eq. (5). For diagnostic purposes, we also use an energy-resolved MSE computed using the optimal alignment for each structure,

$$\text{MSE}^{\text{DOS}}(\mathbf{W}, E) = \frac{1}{N} \sum_A \left( \text{DOS}_A^Q(E + \Delta_A) - \frac{1}{N_A} \sum_{A_i \in A} \text{LDOS}_{A_i}^W(E) \right)^2. \quad (11)$$

For the derived quantities that are independent of the energy reference, namely DOS(E<sub>F</sub>) and  $X(\theta)$ , the quantities are derived from the predicted DOS and compared against that from quantum chemical calculations. As DOS(E<sub>F</sub>) is a scalar quantity, the MSE can be defined as

$$\text{MSE}^{\text{DOS}(E_F)}(\mathbf{W}) = \frac{1}{N} \sum_A (\tilde{y}_A - y_A)^2, \quad (12)$$

where  $\tilde{y}_A$  represents the DOS(E<sub>F</sub>) derived from the predicted DOS of structure A and  $y$  represents the DOS(E<sub>F</sub>) derived from the corresponding quantum chemical calculations. Although  $\tilde{y}_A$  may represent only one point on the predicted DOS spectrum, it depends indirectly from the entire DOS, up to the Fermi level.

Since  $X(\theta)$  is a function of the excitation energy,  $\theta$ , the errors have to be integrated across  $\theta$  as defined in the following,

$$\text{MSE}^X(\mathbf{W}) = \frac{1}{N} \sum_A \int d\theta \left( \tilde{X}_A(\theta) - X_A(\theta) \right)^2. \quad (13)$$

where,  $\tilde{X}_A$  represents the distribution of excitations obtained from the predicted DOS of structure A and  $X_A$  is derived from the corresponding quantum chemical calculation.

With the exception of the Ga<sub>x</sub>As<sub>1-x</sub> dataset, three different energy references, V<sub>H</sub>, E<sub>F</sub>, and the optimizable energy reference, were employed for each dataset and

their results were compared against one another. For the  $\text{Ga}_x\text{As}_{1-x}$  dataset, the  $V_H$  energy reference was not employed due to the wide range of Fermi levels relative to  $V_H$ , at around 24 eV. In order to truncate the DOS energy range at 3 eV above the maximum Fermi Level, the DOS energy range would extend up to 27 eV above the Fermi level for certain structures. Such a wide energy range exceeds the maximum eigenenergy calculated for some structures resulting in an unphysical behaviour, whereby the DOS decays quickly to zero at high energy levels for those structures due to a limitation in the number of bands calculated. Thus, aside from the  $\text{Ga}_x\text{As}_{1-x}$  dataset, a total of 6 different models were trained for each dataset and their performance on the DOS RMSE on the test set are shown in Table I. As the adaptive reference provides the best performance on the secondary quantities for both MLPs and linear models, only the results for the MLPs are shown in Table II while that of the linear models are shown in the Supporting Information.

### C. Discussion

MLPs consistently performed better than linear models in predicting the DOS on the test set (Table I) which is expected considering that MLPs have more parameters and can also capture nonlinear relationships between the features and the DOS. As for the choice of energy reference, the Fermi energy usually leads to smaller RMSE than the average Hartree Potential, which is usually the default choice for most electronic-structure programs. Optimizing the DOS alignment further improves the accuracy, even though the percentage difference in RMSE between the Fermi level energy reference and adaptive reference varies quite significantly across the four datasets. For both the silicon and hydrogen dataset, the improvement in RMSE is rather small at roughly 10%, with larger improvements for MLPs compared to linear models. This is likely due to the high complexity in the dataset in terms of the spectral diversity of the DOS as both datasets contain structures from a wide diversity of phases with few common spectral features to be aligned. Meanwhile, for  $\text{Ga}_x\text{As}_{1-x}$  and  $\text{BaTiO}_3$ , the improvements in RMSE are more significant. For  $\text{Ga}_x\text{As}_{1-x}$ , the improvements are roughly 50% for both types of models while it is 15% and 25% for linear and MLPs respectively on the  $\text{BaTiO}_3$  dataset. Although the  $\text{Ga}_x\text{As}_{1-x}$  and  $\text{BaTiO}_3$  datasets also contain structures of different phases, there are common spectral motifs observed across the dataset. The spectral diversity of each dataset can be seen in Fig. 2, where each panel consists of an overlay of 50 DOS spectrums from the training set. By comparing the panels in the right columns, it can be observed that shared DOS features such as the prominent  $3d$  peaks of gallium and the first two peaks in  $\text{BaTiO}_3$ , become much better aligned under the adaptive reference. Meanwhile, the  $E_F$  energy reference (and  $V_H$  to a larger extent) misaligns these features, in a way that is

not associated with local structural motifs, complicating the learning problem.

Similar trends can be generally observed for the secondary quantities derived from the DOS predictions on the test set. Secondary quantities derived from the predictions of models trained on the adaptive energy reference typically performs the best. The degree of improvement is less significant for silicon and hydrogen while it is usually more prominent for  $\text{Ga}_x\text{As}_{1-x}$  and  $\text{BaTiO}_3$ . Although there were no significant changes in the performance of  $\text{DOS}(E_F)$  for  $\text{Ga}_x\text{As}_{1-x}$ , improvements of roughly 15% can be observed for silicon and hydrogen and  $\text{BaTiO}_3$  exhibits much more prominent improvements at 34% compared to the best performing fixed energy reference. Meanwhile, for the predictions of  $X(\theta)$ , there was a negligible change in performance for hydrogen but there were improvements of 10% of silicon and significantly more improvements for  $\text{Ga}_x\text{As}_{1-x}$  and  $\text{BaTiO}_3$  at 41% and 46%, respectively.

To investigate the model performance at different energy channels, the DOS RMSE was compared energy-wise between MLPs trained using the  $E_F$  and self-aligned energy reference. To calculate the DOS RMSE energy-wise, Eq. (11) was used. The results are shown in Fig. 3 where the vertical axis denotes the change in RMSE, calculated by subtracting the RMSE on the adaptive reference from the RMSE on the Fermi level reference. From the lower quadrants, it can be seen that the improvements in DOS performance when using the adaptive energy reference are most prominent at the energy ranges of common spectral features. This corroborates the previous statement, whereby the misalignment of these features hinders the model performance by further complicating the learning problem. Additionally, in Fig. 4, the histograms of the  $\Delta$  values for the training structures in each dataset also support this interpretation. The two distinct peaks at positive and negative  $\Delta$  for  $\text{BaTiO}_3$  showcase the DOS features moving towards each other. These observations suggest that optimizing the energy reference to improve model performance results in the alignment of common spectral patterns in the dataset. Hence, this accounts for the disparity in improvement in model performance for different datasets, as the effectiveness of the new framework will depend on the degree of similarity in the DOS spectra within the dataset, and on whether one of the common choices of reference leads to substantial shifts of these features in different structures.

## IV. CONCLUSIONS

To conclude, a new DOS learning framework that optimizes the energy reference of each structure has been proposed. The performance of the new framework was compared against two conventional energy alignment approaches: the mean Hartree potential and the Fermi energy. Across four datasets, models trained under the new framework consistently outperforms others in terms of

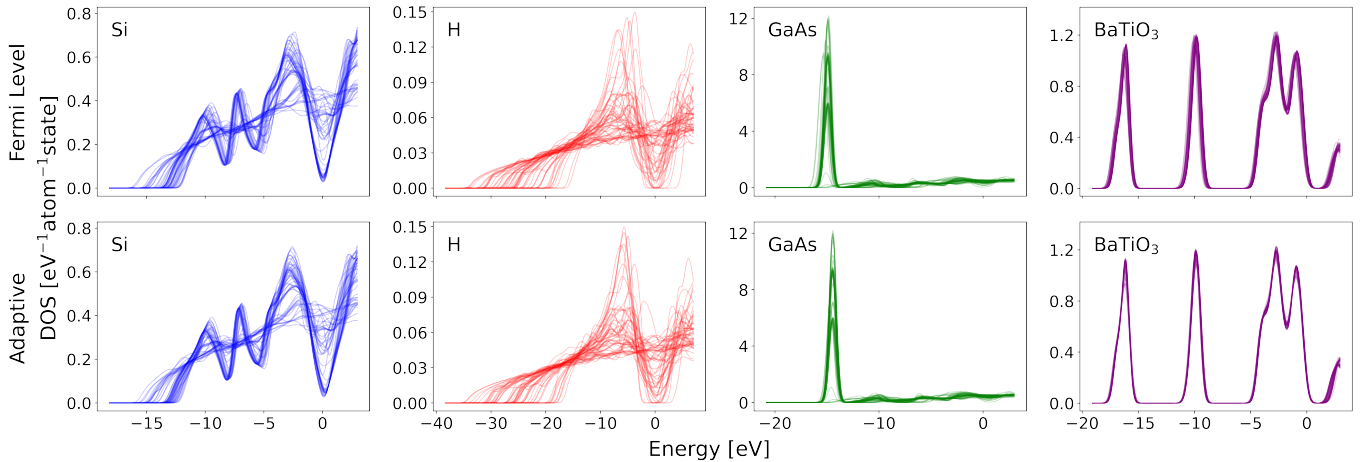


FIG. 2. DOS overlay plots of each dataset with different energy references is shown in each panel. Each overlay plot contains 50 different lines, corresponding to the DOS of 50 different structures in each dataset as indicated in each panel. The top row of the figure depicts the DOSes with the energy reference set to the Fermi level while the lower row depicts the DOSes using the adaptive energy reference.

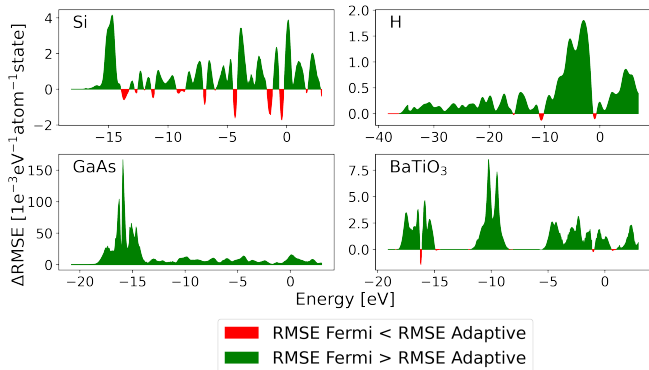


FIG. 3. Difference in energy-wise DOS RMSE for the MLP models trained using the Fermi level versus the adaptive energy reference for the dataset. Green regions indicate where the model trained on the adaptive energy reference performs better, while red regions indicate that the Fermi level energy reference perform better. It can be seen that models trained on the adaptive energy reference outperform those referenced to the Fermi level across the majority of the energy range.

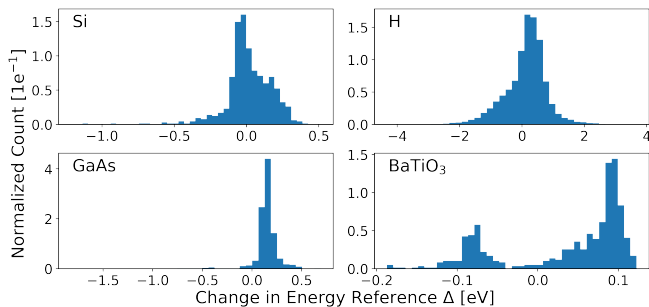


FIG. 4. Histogram of  $\Delta$  for the training structures for each dataset for MLPs. The histograms are normalized with respect to the sizes of the training set to make the sum of all bins equal to 1.

the DOS and its derived quantities. Additionally, some justification behind the optimization process is provided. Energy ranges in the DOS that experience the greatest improvement in performance contain common spectral patterns that are shared across the dataset and the optimization process works to align them. Hence, the approach is likely to provide the best increase in performance when dealing with datasets whereby there are significant regions of the DOS that remain constant across the structures, but are rigidly shifted when using conventional energy references. More generally, this work highlights the significance and the benefits of defining evaluation metrics in a manner that is consistent with the physics of the problem. For instance, the concept of optimizing an internal or ill-defined reference can be readily applied to applications outside of the DOS. To give a few examples, this approach can also be easily extended to the optimization of the energy reference for the prediction of the spatially resolved density of states. Additionally, it can also be applied to the prediction of the Hamiltonian of bulk structures [53, 54], whereby the eigenvalues obtained from the Hamiltonian do not have a well defined external energy reference.

## ACKNOWLEDGMENTS

The authors would like to thank Chiheb Ben Mahmoud for support during the early implementation of the method. MC and SC acknowledge support by the Swiss National Science Foundation (Project 200020\_214879). WBH and MC acknowledge support by the MARVEL National Centre of Competence in Research (NCCR), funded by the Swiss National Science Foundation (grant agreement ID 51NF40-182892). FG and MC acknowledge funding from the European Research Council

(ERC) under the European Union’s Horizon 2020 research and innovation programme Grant No. 101001890-FIAMMA. FG also acknowledges funding from the Euro-

pean Union’s Horizon 2020 research and innovation programme under the Marie Skłodowska-Curie Action IF-EF-ST, grant agreement No. 101018557-TRANQUIL.

- 
- [1] M. Y. Toriyama, A. M. Ganose, M. Dylla, S. Anand, J. Park, M. K. Brod, J. M. Munro, K. A. Persson, A. Jain, and G. J. Snyder, *Materials Today Electronics* **1**, 100002 (2022).
- [2] N. W. Ashcroft and N. D. Mermin, *Solid State Physics* (Holt, Rinehart and Winston, 1976) google-Books-ID: 1C9HAQAAIAAJ.
- [3] A. Chandrasekaran, D. Kamal, R. Batra, C. Kim, L. Chen, and R. Ramprasad, *npj Computational Materials* **5**, 1 (2019).
- [4] M. Ceriotti, C. Clementi, and O. Anatole von Lilienfeld, *The Journal of Chemical Physics* **154**, 160401 (2021).
- [5] O. V. Prezhdo, *The Journal of Physical Chemistry Letters* **11**, 9656 (2020).
- [6] F. Noé, A. Tkatchenko, K.-R. Müller, and C. Clementi, *Annual Review of Physical Chemistry* **71**, 361 (2020).
- [7] I. Poltavsky and A. Tkatchenko, *The Journal of Physical Chemistry Letters* **12**, 6551 (2021).
- [8] R. Ramprasad, R. Batra, G. Pilania, A. Mannodi-Kanakithodi, and C. Kim, *npj Computational Materials* **3**, 54 (2017).
- [9] F. Musil, A. Grisafi, A. P. Bartók, C. Ortner, G. Csányi, and M. Ceriotti, *Chemical Reviews* **121**, 9759 (2021).
- [10] A. Glielmo, B. E. Husic, A. Rodriguez, C. Clementi, F. Noé, and A. Laio, *Chemical Reviews* **121**, 9722 (2021).
- [11] J. Nigam, M. J. Willatt, and M. Ceriotti, *The Journal of Chemical Physics* **156**, 014115 (2022).
- [12] K. K. Huguenin-Dumittan, P. Loche, N. Haoran, and M. Ceriotti, *The Journal of Physical Chemistry Letters* **14**, 9612 (2023), publisher: American Chemical Society.
- [13] R. Drautz, *Physical Review B* **99**, 014104 (2019), publisher: American Physical Society.
- [14] A. P. Bartók, R. Kondor, and G. Csányi, *Physical Review B* **87**, 184115 (2013).
- [15] K. T. Schütt, P.-J. Kindermans, H. E. Saucedo, S. Chmiela, A. Tkatchenko, and K.-R. Müller, arXiv:1706.08566 [physics, stat] (2017), arXiv: 1706.08566.
- [16] S. N. Pozdnyakov and M. Ceriotti, (2024).
- [17] N. Lee, H. Noh, S. Kim, D. Hyun, G. S. Na, and C. Park, “Predicting Density of States via Multimodal Transformer,” (2023), arXiv:2303.07000 [cond-mat, physics:physics].
- [18] S. Chong, F. Grasselli, C. Ben Mahmoud, J. D. Morrow, V. L. Deringer, and M. Ceriotti, *Journal of Chemical Theory and Computation* **19**, 8020 (2023), publisher: American Chemical Society.
- [19] B. Kailkhura, B. Gallagher, S. Kim, A. Hiszpanski, and T. Y.-J. Han, *npj Computational Materials* **5**, 1 (2019), publisher: Nature Publishing Group.
- [20] W. B. How, B. Wang, W. Chu, A. Tkatchenko, and O. V. Prezhdo, *The Journal of Physical Chemistry Letters* , 12026 (2021).
- [21] W. B. How, B. Wang, W. Chu, S. M. Kovalenko, A. Tkatchenko, and O. V. Prezhdo, *The Journal of Chemical Physics* **156**, 054110 (2022).
- [22] A. Kabylda, V. Vassilev-Galindo, S. Chmiela, I. Poltavsky, and A. Tkatchenko, *Nature Communications* **14**, 3562 (2023), publisher: Nature Publishing Group.
- [23] Y. Zhu, J. Peng, X. Kang, C. Xu, and Z. Lan, *Physical Chemistry Chemical Physics* **24**, 24362 (2022), publisher: Royal Society of Chemistry.
- [24] N. Lopanitsyna, G. Fraux, M. A. Springer, S. De, and M. Ceriotti, *Physical Review Materials* **7**, 045802 (2023), publisher: American Physical Society.
- [25] J. Behler and M. Parrinello, *Physical Review Letters* **98**, 146401 (2007).
- [26] S. R. Broderick and K. Rajan, *EPL (Europhysics Letters)* **95**, 57005 (2011).
- [27] B. C. Yeo, D. Kim, C. Kim, and S. S. Han, *Scientific Reports* **9**, 5879 (2019).
- [28] K. Bang, B. C. Yeo, D. Kim, S. S. Han, and H. M. Lee, *Scientific Reports* **11**, 11604 (2021), number: 1 Publisher: Nature Publishing Group.
- [29] B. G. del Rio, C. Kuenneth, H. D. Tran, and R. Ramprasad, *The Journal of Physical Chemistry A* **124**, 9496 (2020).
- [30] V. Fung, G. Hu, P. Ganesh, and B. G. Sumpter, *Nature Communications* **12**, 88 (2021), number: 1 Publisher: Nature Publishing Group.
- [31] S. Kong, F. Ricci, D. Guevarra, J. B. Neaton, C. P. Gomes, and J. M. Gregoire, *Nature Communications* **13**, 949 (2022), number: 1 Publisher: Nature Publishing Group.
- [32] C. Ben Mahmoud, A. Anelli, G. Csányi, and M. Ceriotti, *Physical Review B* **102**, 235130 (2020).
- [33] A. Zunger and M. L. Cohen, *Physical Review B* **18**, 5449 (1978).
- [34] V. Blum, R. Gehrke, F. Hanke, P. Havu, V. Havu, X. Ren, K. Reuter, and M. Scheffler, *Computer Physics Communications* **180**, 2175 (2009).
- [35] L. Kleinman, *Physical Review B* **24**, 7412 (1981).
- [36] A. J. Logsdail, D. O. Scanlon, C. R. A. Catlow, and A. A. Sokol, *Physical Review B* **90**, 155106 (2014).
- [37] K. T. Butler, C. H. Hendon, and A. Walsh, *Journal of the American Chemical Society* **136**, 2703 (2014), publisher: American Chemical Society.
- [38] D. O. Scanlon, C. W. Dunnill, J. Buckeridge, S. A. Shevlin, A. J. Logsdail, S. M. Woodley, C. R. A. Catlow, M. J. Powell, R. G. Palgrave, I. P. Parkin, G. W. Watson, T. W. Keal, P. Sherwood, A. Walsh, and A. A. Sokol, *Nature Materials* **12**, 798 (2013), publisher: Nature Publishing Group.
- [39] A. Baldereschi, S. Baroni, and R. Resta, *Physical Review Letters* **61**, 734 (1988).
- [40] E. Catmull and R. Rom, in *Computer Aided Geometric Design*, edited by R. E. Barnhill and R. F. Riesenfeld (Academic Press, 1974) pp. 317–326.
- [41] A. P. Bartók, J. Kermode, N. Bernstein, and G. Csányi, *Physical Review X* **8**, 041048 (2018).

- [42] B. Cheng, G. Mazzola, C. J. Pickard, and M. Ceriotti, *Nature* **585**, 217 (2020), publisher: Nature Publishing Group.
- [43] P. Giannozzi, O. Andreussi, T. Brumme, O. Bunau, M. Buongiorno Nardelli, M. Calandra, R. Car, C. Cavazzoni, D. Ceresoli, M. Cococcioni, N. Colonna, I. Carnimeo, A. Dal Corso, S. De Gironcoli, P. Delugas, R. A. DiStasio, A. Ferretti, A. Floris, G. Fratesi, G. Fugallo, R. Gebauer, U. Gerstmann, F. Giustino, T. Gorni, J. Jia, M. Kawamura, H.-Y. Ko, A. Kokalj, E. Küçükbenli, M. Lazzeri, M. Marsili, N. Marzari, F. Mauri, N. L. Nguyen, H.-V. Nguyen, A. Otero-de-la Roza, L. Paulatto, S. Poncé, D. Rocca, R. Sabatini, B. Santra, M. Schlipf, A. P. Seitsonen, A. Smogunov, I. Timrov, T. Thonhauser, P. Umari, N. Vast, X. Wu, and S. Baroni, *Journal of Physics: Condensed Matter* **29**, 465901 (2017).
- [44] P. Giannozzi, O. Baseggio, P. Bonfà, D. Brunato, R. Car, I. Carnimeo, C. Cavazzoni, S. De Gironcoli, P. Delugas, F. Ferrari Ruffino, A. Ferretti, N. Marzari, I. Timrov, A. Urru, and S. Baroni, *The Journal of Chemical Physics* **152**, 154105 (2020).
- [45] P. Giannozzi, S. Baroni, N. Bonini, M. Calandra, R. Car, C. Cavazzoni, D. Ceresoli, G. L. Chiarotti, M. Cococcioni, I. Dabo, A. Dal Corso, S. De Gironcoli, S. Fabris, G. Fratesi, R. Gebauer, U. Gerstmann, C. Gougoussis, A. Kokalj, M. Lazzeri, L. Martin-Samos, N. Marzari, F. Mauri, R. Mazzarello, S. Paolini, A. Pasquarello, L. Paulatto, C. Sbraccia, S. Scandolo, G. Sclauzero, A. P. Seitsonen, A. Smogunov, P. Umari, and R. M. Wentzcovitch, *Journal of Physics: Condensed Matter* **21**, 395502 (2009).
- [46] C. Ben Mahmoud, F. Grasselli, and M. Ceriotti, *Physical Review B* **106**, L121116 (2022).
- [47] A. Karvounis, F. Timpu, V. V. Vogler-Neuling, R. Savo, and R. Grange, *Advanced Optical Materials* **8**, 2001249 (2020), eprint: <https://onlinelibrary.wiley.com/doi/pdf/10.1002/adom.202001249>.
- [48] B. Ertuğ, *American Journal of Engineering Research* (2013).
- [49] L. Gigli, M. Veit, M. Kotiuga, G. Pizzi, N. Marzari, and M. Ceriotti, *npj Computational Materials* **8**, 1 (2022), number: 1 Publisher: Nature Publishing Group.
- [50] P. A. Verrinder, L. Wang, J. Fridlander, F. Sang, V. Rosborough, M. Nickerson, G. Yang, M. Stephen, L. Coldren, and J. Klamkin, *IEEE Journal of Selected Topics in Quantum Electronics* **28**, 1 (2022), conference Name: *IEEE Journal of Selected Topics in Quantum Electronics*.
- [51] Z. Li, T. H. Kim, S. Y. Han, Y. Yun, S. Jeong, B. Jo, S. A. Ok, W. Yim, S. H. Lee, K. Kim, S. Moon, J. Park, T. K. Ahn, H. Shin, J. Lee, and H. J. Park, *Advanced Energy Materials* **10**, 1903085 (2020).
- [52] G. Imbalzano and M. Ceriotti, *Physical Review Materials* **5**, 063804 (2021).
- [53] Y. Zhong, H. Yu, J. Yang, X. Guo, H. Xiang, and X. Gong, “Universal Machine Learning Kohn-Sham Hamiltonian for Materials,” (2024), version Number: 2.
- [54] H. Li, Z. Wang, N. Zou, M. Ye, R. Xu, X. Gong, W. Duan, and Y. Xu, (2021), 10.48550/ARXIV.2104.03786, publisher: arXiv Version Number: 2.